Conditional π -Phase Shift of Single-Photon-Level Pulses at Room Temperature

Steven Sagona-Stophel[®], *,[‡] Reihaneh Shahrokhshahi, [‡] Bertus Jordaan, Mehdi Namazi, and Eden Figueroa [†] Department of Physics and Astronomy, Stony Brook University, Stony Brook, New York 11794-3800, USA

(Received 28 June 2019; accepted 15 October 2020; published 8 December 2020)

The development of useful photon-photon interactions can trigger numerous breakthroughs in quantum information science, however, this has remained a considerable challenge spanning several decades. Here, we demonstrate the first room-temperature implementation of large phase shifts ($\approx \pi$) on a single-photon level probe pulse (1.5 μ s) triggered by a simultaneously propagating few-photon-level signal field. This process is mediated by Rb⁸⁷ vapor in a double- Λ atomic configuration. We use homodyne tomography to obtain the quadrature statistics of the phase-shifted quantum fields and perform maximum-likelihood estimation to reconstruct their quantum state in the Fock state basis. For the probe field, we have observed input-output fidelities higher than 90% for phase-shifted output states, and high overlap (over 90%) with a theoretically perfect coherent state. Our noise-free, four-wave-mixing-mediated photon-photon interface is a key milestone toward developing quantum logic and nondemolition photon detection using schemes such as coherent photon conversion.

DOI: 10.1103/PhysRevLett.125.243601

Photons are primordial for transmitting [1,2] and storing [3–5] quantum information. Additionally, there exist photon-based quantum processing applications such as, quantum random access memory [6] and quantum machine learning [7]. The cornerstone of this "photonic processing" is a photon-photon phase gate [8]. However, its experimental realization has a number of challenges: (i) a system must exhibit large cross-phase modulation (XPM) such that a single photon causes a π phase shift on a second photon state, (ii) the quantum state of the output must not be distorted and, (iii) a "truth table" of input combinations must be achieved with high fidelity.

Cavity-based and Rydberg-based systems have demonstrated large XPM at the single-photon level [9–11], and have begun investigating fidelities of a photon-photon gate [12,13]. However, these new schemes need cavities or require the light to be stored in an atomic medium, which dramatically lowers the gate's efficiency, ranging from 0.5% to 8%, with an entangling gate fidelity of $63.7\% \pm 4.5\%$ [13]. Therefore, further advances need to be made before these systems are ready for large problems requiring fault tolerance [14].

Additionally, it has recently been shown that, unlike previously thought [15,16], there are indeed nonlinear systems that are capable of large phase shifts at high fidelity [17], and they can perform gate operations even in a full frequency-mode framework [18]. These systems use a paradigm called "coherent photon conversion" (CPC) [19], using four-wave mixing (FWM). Combined with linear optics, these processes can form the basis for universal quantum computation [20].

A quantum photonic gate using CPC requires (i) FWM for single photon inputs, (ii) an output quantum state with

low-noise in the Fock state basis, (iii) the two photon inputs must be efficiently converted into a third (initially vacuum) field and then converted back, thereby creating a "Rabi oscillation" between the $|1,1,0\rangle$ and $|0,0,1\rangle$ states [19].

While current work toward CPC uses nonlinear waveguides and is limited by the efficiency of the quantum process [21], atomic systems can create FWM [22] at near unitary efficiencies, and are an excellent candidate for highly efficient CPC. Additionally, it has been shown that using FWM systems, it is possible to achieve large XPM at the low light level without requiring cavities, storage or Rydberg levels [23].

In this experiment we demonstrate the first room-temperature implementation of a single-photon level FWM double- Λ system (DL) in which simultaneously propagating pulses of single-photon-level light create π phase shifts. We perform a quantum characterization of these phase-shifted output states using quantum state tomography of the quadrature statistics. We also show that four-wave mixing processes at room temperature produce well-behaved quantum states, observing high fidelities for single-photon level light phase shifted by π .

We use a double- Λ atomic system in a room-temperature Rb⁸⁷ atomic ensemble, in which both individual Λ subsystems exhibit electromagnetically induced transparency (EIT) [see Supplemental Material (SM) for experimental details [24]]. As illustrated in Fig. 1(b), we send a pulse sequence consisting of three cases: probe pulse only, probe and signal pulse on (creating the double- Λ system), and signal only (generating FWM). Each pulse is 1.5 μ s long, each case is separated with a 20 μ s interpulse delay, and this is repeated every 60 μ s. Control fields 1 and 2 are on during the whole cycle.

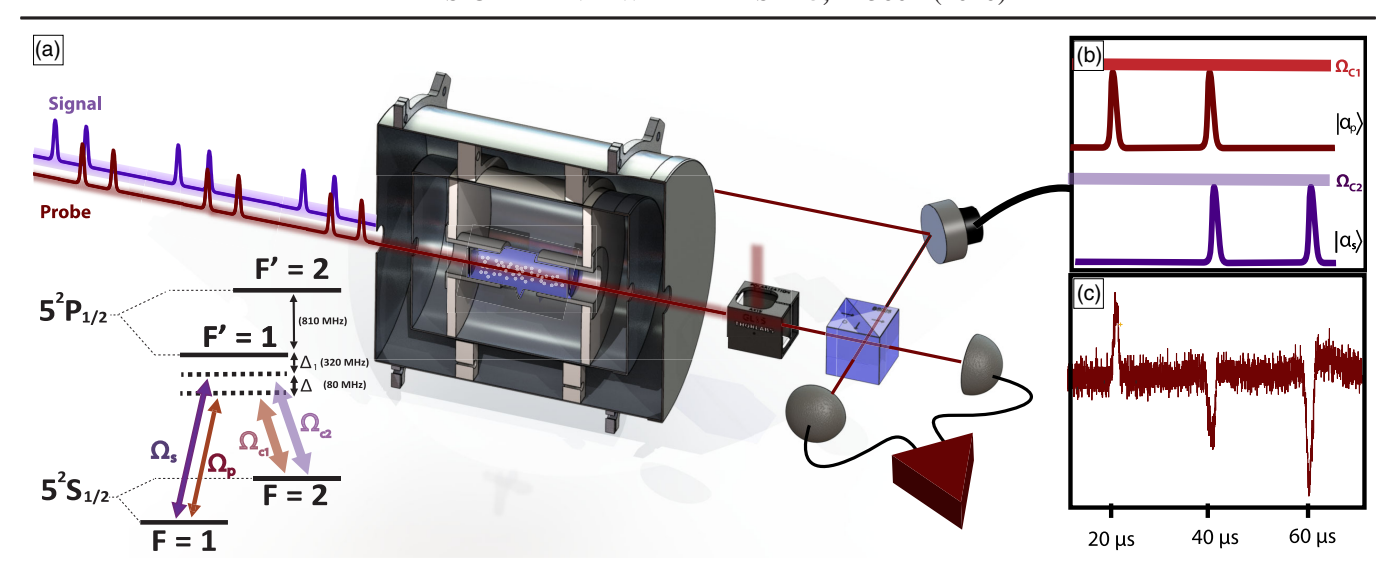


FIG. 1. (a) Experimental setup. A sequence of probe (Ω_p) and signal pulses (Ω_s) are sent through a room-temperature ⁸⁷Rb atomic ensemble. The probe output is then measured on a balanced homodyne detector and the associated quadrature and phase values are analyzed. (b) Diagram of our sequence of input pulses. First, we send a pulsed probe field (Ω_p) , with two CW control fields $(\Omega_{c1}, \Omega_{c2})$ creating EIT. Second, we add a pulsed signal Ω_s field (in addition to the probe Ω_p pulse), creating a double- Λ system. Third, we switch off the probe pulse (leaving the signal pulse on), creating four-wave mixing FWM in the frequency of the probe. (c) Voltage values of the balanced homodyne detector, representing quadrature measurements of the pulse sequence. Across a scan of the phase of the local oscillator of the homodyne, phase information can be extracted from these pulses (as discussed in the SM [24]).

A key feature of this double- Λ system is that the output FWM-assisted phase shift is phase sensitive on the input phases of multiple fields [41]. Accordingly, we identify an important parameter for our experiment: $\Delta\phi_{\rm FWM} \equiv \phi_{\rm FWM}^p - \phi_{\rm PO}^p$, which represents the relative phase between the generated FWM and the "probe-only" case. This phase sensitivity of the FWM is a critical feature because the output light's amplitude $E_p^{\rm DL}(\Delta\phi_{\rm FWM})$ and phase shift (written as $\Delta\phi_{\rm DL}$) are both functions of $\Delta\phi_{\rm FWM}$ (see SM for full dependence [24]).

We use a standard balanced homodyne detector to obtain accurate phase and quadrature information of the phaseshifted double- Λ system output. We estimate $\Delta\phi_{\rm FWM}$ and $\Delta \phi_{\rm DL}$ simultaneously by implementing a closely separated three pulse sequence with a fast local oscillator scan (illustrated in Fig. S2a [24]). We let the interferometric phases fluctuate randomly and we collect quadrature statistics of the output double-A system and bin them by the phase shift that uniquely describes their state ($\Delta \phi_{\rm FWM}$). Additionally, we also collect quadrature data describing the quantum states of the light generated by the FWM and the probe light experiencing EIT-like behavior. Furthermore, the data across multiple local oscillator scans is evaluated using maximum-likelihood estimation to uncover their quantum states in the Fock state basis [42,43]. This workflow of this data processing is illustrated in Fig. S2.

When using coherent states as inputs, our theoretical model predicts the obtained phase shifts to be the result of a linear interference of a probe-only contribution and "FWM" contribution. Using the approximations that

$$\begin{split} \Delta_p &= \Delta_{c1} = \Delta \text{ (the detuning of the probe and the first control field), } \Delta_s = \Delta_{c2} = 3\Delta \text{ (signal and second control field detunings), and } \gamma = 0 \text{ (decoherence between ground states), our double-} \Lambda \text{ output field } E_p^{DL} \text{ has the form } E_p^{DL} = \underbrace{(\Omega_{c1}^2 + \Omega_{c2}^2 e^{f_p}/\Omega_{c1}^2 + \Omega_{c2}^2)|E_p^{in}|}_{\text{probe-onlycontribution}} - \end{split}$$

$$\underbrace{(\Omega_{c1}\Omega_{c2}(e^{f_s}-1)/\Omega_{c1}^2+\Omega_{c2}^2)|E_s^{\rm in}|e^{i\Delta\phi_4}}_{\text{four-wave-mixing contribution}}.$$

$$\begin{split} f_s &= -\frac{kz\sqrt{\pi\log(2)}(\Omega_{c1}^2 + \Omega_{c2}^2)}{\Gamma(\Omega_{c1}^2 + \Omega_{c2}^2) - 2i\Delta(3\Omega_{c1}^2 + \Omega_{c2}^2) + 2W(\Omega_{c1}^2 + \Omega_{c2}^2)}, \\ f_p &= -\frac{kz\sqrt{\pi\log(2)}(\Omega_{c1}^2 + \Omega_{c2}^2)}{\Omega_{c1}^2(\Gamma - 6i\Delta + 2W) + \Omega_{c2}^2(\Gamma - 2i\Delta + 2W)}, \end{split}$$

where $\Omega_{p,sc1,c2}$ are the Rabi frequencies of the probe, signal, and the two control fields. Additionally, $k = (\alpha \gamma / 2L\wp)$, Γ is the decay rate, W is a parameter describing Doppler width of our atomic ensemble, α is the optical depth, L is the length of the cell, \wp is the dipole moment element (see SM for full derivation [24]).

Using this result, we introduce an effective photonphoton model and find the expected value of the quadrature values $X(\theta)_p^{\rm DL}$ of the DL output:

$$\begin{split} \langle \alpha_{s} | \langle \alpha_{p} | X(\theta)_{p}^{\text{DL}} | \alpha_{p} \rangle | \alpha_{s} \rangle \\ &= \sqrt{2} [|\alpha_{\text{PO}}| \cos(\theta) + |\alpha_{\text{FWM}}| \cos(\Delta \phi_{\text{FWM}} - \theta)], \end{split}$$

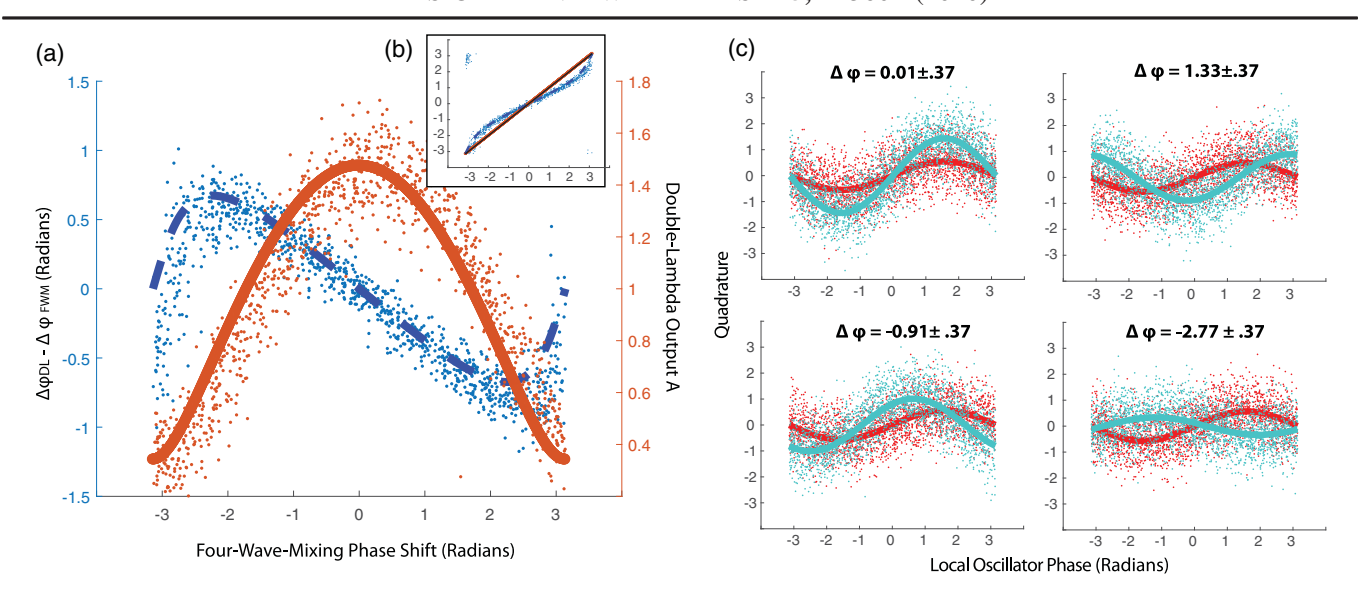


FIG. 2. (a),(b) Comparison between the phase and amplitude of each sinusoidal fit of individual homodyne scans and theoretical values for single-photon-level data. (a) The blue dots represent individual values of $\Delta\phi_{\rm DL} - \Delta\phi_{\rm FWM}$ vs $\Delta\phi_{\rm FWM}$ for each individual homodyne "scan." The orange dots represent the fitted amplitudes, $A(\alpha_{\rm FWM}, \alpha_p, \Delta\phi_{\rm FWM})$, of each homodyne shot for the DL case. These are compared to their theoretical values (solid orange and dashed blue lines) obtained from Eqs. (21) and (22) in the SM, with $\alpha_p = 0.57$ and $\alpha_{\rm FWM} = 0.91$ [24]. No free parameters are used in the theoretical fits. In (b) the blue points represent the phase shift, $\Delta\phi_{\rm DL}$ vs $\Delta\phi_{\rm FWM}$. Part (c), to reconstruct the quantum state, the quadrature statistics obtained from the outputs must be sorted by their associated $\Delta\phi_{\rm FWM}$ phase shifts. Using the phase information illustrated in (a) and (b), we can collect quadrature statistics associated with different binned phases (as discussed in the SM [24]). Extracted single-photon-level quadrature data are illustrated for the double- Δ (teal) and EIT reference (red)—for different sets of postselected phase shifts (for bins $\Delta\phi_{\rm FWM} \in 0.01, 1.33, -0.91$, and -2.77 ± 0.37 radians). Quadrature values are compared to their averaged fitted values (plotted as a solid line in red and teal).

where α_{PO} and α_{FWM} are the coherent-state amplitudes for the probe-only and FWM cases and θ is the phase of the local oscillator. The theoretical DL amplitude vs $\Delta\phi_{FWM}$ is visualized as the solid orange line in Fig. 2(a), while the dashed blue line in Fig. 2(b) represents $\Delta\phi_{DL}$ vs $\Delta\phi_{FWM}$. This simple model matches the experimental data without any free parameters at the single-photon level. The small degree of uncertainty in the experimental estimation of our phases ($\Delta\phi_{FWM}$ and $\Delta\phi_{DL}$) implies we can accurately associate quadrature statistics with a particular phase-shifted output state, thereby allowing accurate quantum state estimation through binning.

For each sweep of the homodyne local oscillator phase, an accurate value of the output phase shift $\Delta\phi_{\rm DL}$ and the four-wave mixing phase shift $\Delta\phi_{\rm FWM}$ can be extracted from the peaks of the pulses (as illustrated in the SM, Fig. S2, part b [24]). Therefore, for every output phase shift (represented by a single data point in Fig. S2, part c), we obtain an entire set of homodyne statistics $\{X(\theta)\}$, all associated with a particular FWM phase shift $\Delta\phi_{\rm FWM}$. We then organize the output phase shifts into ten bins and combine the quadrature sets $\{X(\theta)\}$ with their associated FWM phase shifts in the same the bin region. A selection of these combined sets is plotted in Fig. 2(c).

For each combined set (binned by $\Delta\phi_{\rm FWM}$), we perform a quantum state reconstruction for each case: probe only, double- Λ , and FWM. Additionally, we also measure and

reconstruct the density matrix for the probe and signal fields without the cell. The reconstructed density matrices can additionally be mapped to a Wigner function representation for easier visualization. Figure 3 illustrates an input-output representation for different phase-shifted output states, while Fig. 4(a) shows how both the four-wave mixing and the double- Λ system traverse phase space. In Fig. 4(a), we observe an unshifted circle (in dark blue) representing the maximum values of each Wigner function of the four-wave mixing in phase space, indicating the mean photon number of the quantum state of the FWM does not change with phase. This is unlike the double- Λ system which has its maximum values in phase space represented by a shifted circle (illustrated in teal), as expected by our theoretical model.

To better understand and characterize our system using the reconstructed density matrices we calculate two values, which we name the "coherent-state fidelity" (CSF) and the "phase-aligned, input-output fidelity" (PAIOF). The CSF, which measures the fidelity between our state and a theoretical coherent state of the same mean photon number and phase, is useful for characterizing changes due to noise or unwanted nonlinear processes. As shown in Fig. 4(c), we find that our phase-shifted states retain a remarkably high CSF at the single-photon level—remaining above 90%. These values reach as high as $94.4\% \pm 0.5\%$ for the bin $\Delta\phi_{\rm FWM} \in (1.69, 2.43)$ radians, a surprising result

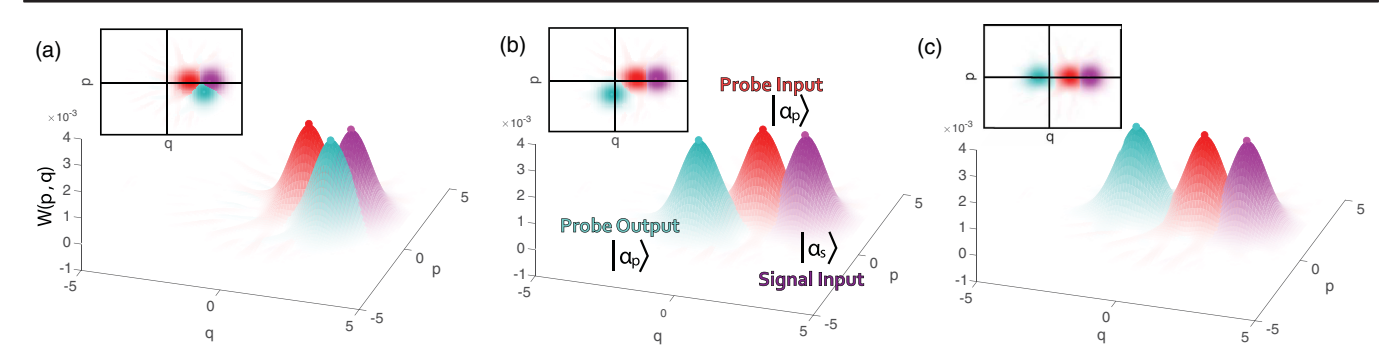


FIG. 3. Reconstructed density matrices represented as Wigner functions are plotted, illustrating the relationship between inputs and outputs for different postselected phase shifts. The red and purple plots are the input states of the probe and signal. The teal plot is the phase-shifted probe output for (a) 0.3 radians phase shift, (b) $\pi/2$ phase shift, and (c) π phase shift.

considering that thermal noise typically affects output fidelities in storage of light in similar systems. We also calculate the purity operator ρ^2 . For the DL system exhibiting large phase shifts [within the bin $\Delta\phi_{\rm FWM} \in (2.42,3.14)$ radians], we observe a purity of 0.92 ± 0.02 , as compared to a purity of 0.93 ± 0.01 for the EIT-like case and 0.96 ± 0.02 for the FWM-only case. This high level of purity and coherent-state fidelity indicates that we are measuring neither large amounts of parasitic thermal light nor decoherence in our phase-shift process (from, for example, thermal or Doppler effects). The results are consistent with a simple quantum model which takes

Doppler-broadening into account (described in the SM [24]). Additionally, since these values are not unitary, we also describe in the SM various sources that could cause quantum damage [24]. Overall, we attribute most of this "damage" to statistical errors in the reconstruction.

Since the CSF does not characterize overall losses due to attenuation, we use the phase-aligned, input-output fidelity (PAIOF) to characterize these losses. This value compares the overlap between the input state and the output state with a modified phase that is aligned in phase with the input state. Using the quantum state of the light without the cell, $\rho_{\text{in}_{\theta}}$, and a double- Λ output with a

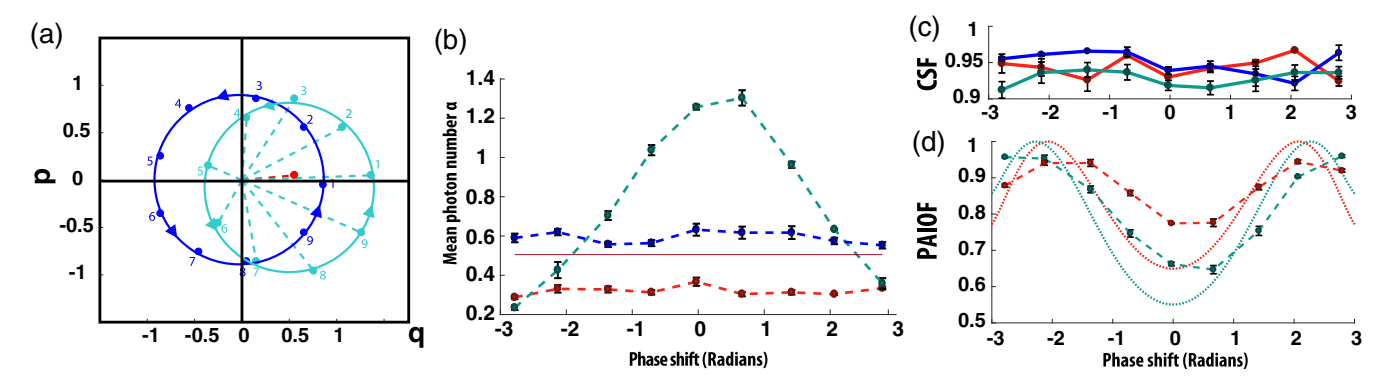


FIG. 4. (a) For each postselected phase bin, the position in the phase space where the Wigner functions exhibit their maximum values are plotted, illustrating the motion in phase space of the probe output as the global input phase is changed. These maxima are illustrated for the double-Λ states (in teal) and the four-wave mixing (in blue). Additionally, the maximum for the probe-only case is labeled in red for comparison. (b) Plots of mean photon number from reconstructed states, as a function of postselected phase shifts. Photon numbers are plotted as dashed lines for double-Λ (dashed teal), four-wave mixing (dashed blue), EIT-probe (dashed red), and probe input (solid red). (c) Plots of "coherent-state fidelity" (CSF) from reconstructed states, as a function of postselected phase shifts. For each postselected phase shift, the associated reconstructed state is compared to a theoretical, perfect coherent state of the same mean photon number and phase. This is done for quadrature statistics for each pulse sequence (probe-only, double-Λ system, and FWM in red, teal, and blue, respectively). (d) Plots of "phase-aligned, input-output fidelity" (PAIOF) from reconstructed states as a function of postselected phase shifts. The PAIOF fidelity (plotted as a dashed red line) is found by comparing the density matrix overlap between a reference in which the probe is reconstructed without the Rb cell and the phase-shifted double-Λ output state. In calculating the PAIOF, the phase of double-Λ state is shifted to be aligned to the phase of the input. Additionally, a "phase-aligned fidelity" is calculated between reconstructed states obtained between the pulse sequence 1 (probe-only case) and the pulse sequence 2 (double-Λ case) and is plotted as a dashed green line. For comparison, we additionally plot the same phase-aligned fidelity calculations with theoretically perfect coherent states with the same mean photon number (as dotted red and green lines).

modified phase, notated as $\rho_{\mathrm{DL}_{\theta_0}}$, we define the PAIOF as $F_{\theta} \equiv (\mathrm{tr} \sqrt{\sqrt{\rho_{\mathrm{in}_{\theta}}} \rho_{\mathrm{DL}_{\theta_0}} \sqrt{\rho_{\mathrm{in}_{\theta}}}})^2$. The PAIOF is plotted as a function of phase shift in Fig. 4(d) as a dashed red line. This value reaches its highest value of 94.4% \pm 0.5% for the bin $\Delta\phi_{\mathrm{FWM}} \in (1.69, 2.43)$ radians, indicating that large phase shifts can be obtained without substantial losses.

Our results demonstrate that protocols utilizing effective single-photon-level FWM processes in Rb cells are achievable, despite their room-temperature operation. This bodes well for the future construction of FWM-mediated quantum nonlinear systems.

We mention that in its current form, our double- Λ system cannot form a full truth table necessary for quantum logic, because the "phase-triggering" photon $|1\rangle_s$ is partially converted into the other frequency mode $|\alpha_p\rangle$, which lowers the fidelity of the desired output state (see Sec. XI in SM [24]). Despite this, the well-behaved nature of the analyzed quantum states demonstrates that near-resonant atomic systems are a viable candidate for a future gate using CPC. As the primary mechanism creating the phase-shifted light in this double-Λ system is two interfering four-wavemixing channels, we have positively checked the first two benchmarks for implementation of the CPC protocol, as outlined in the introduction. Observing no detrimental effects on fidelity of the quantum state of these 1-to-1 photon processes indicates that this architecture is ready to explore 1-to-2 photon conversion necessary for CPC [19]. This would give our system the potential to achieve 2-qubit gate operations and quantum nondemolition measurements of single photons.

We thank Julio Gea Banacloche, Bing He, Balakrishnan Viswanathan, and Aephraim Steinberg for enlightening discussions. The work was supported by the U.S.-Navy Office of Naval Research, Grant No. N00141410801, the National Science Foundation, Grants No. PHY-1404398 and No. PHY-1707919 and the Simons Foundation, Grant No. SBF241180. B. J. acknowledges financial assistance of the National Research Foundation (NRF) of South Africa. S. S. acknowledges financial assistance of the United States Department of Education through a GAANN Fellowship P200A150027-17.

- [3] Y. Wang, M. Um, J. Zhang, S. An, M. Lyu, J.-N. Zhang, L.-M. Duan, D. Yum, and K. Kim, Single-qubit quantum memory exceeding ten-minute coherence time, Nat. Photonics 11, 646 (2017).
- [4] W. Zhang, D.-S. Ding, Y.-B. Sheng, L. Zhou, B.-S. Shi, and G.-C. Guo, Quantum Secure Direct Communication with Quantum Memory, Phys. Rev. Lett. **118**, 220501 (2017).
- [5] A. I. Lvovsky, B. C. Sanders, and W. Tittel, Optical quantum memory, Nat. Photonics 3, 706 (2009).
- [6] J. Biamonte, P. Wittek, N. Pancotti, P. Rebentrost, N. Wiebe, and S. Lloyd, Quantum machine learning, Nature (London) 549, 195 (2017).
- [7] N. Killoran, T. R. Bromley, J. M. Arrazola, M. Schuld, N. Quesada, and S. Lloyd, Continuous-variable quantum neural networks, Phys. Rev. Research 1, 033063 (2019).
- [8] I. L. Chuang and Y. Yamamoto, Simple quantum computer, Phys. Rev. A 52, 3489 (1995).
- [9] D. Tiarks, S. Schmidt, G. Rempe, and S. Dürr, Optical π phase shift created with a single-photon pulse, Sci. Adv. 2, e1600036 (2016).
- [10] K. M. Beck, M. Hosseini, Y. Duan, and V. Vuletić, Large conditional single-photon cross-phase modulation, Proc. Natl. Acad. Sci. U.S.A. 113, 9740 (2016).
- [11] A. Feizpour, M. Hallaji, G. Dmochowski, and A.M. Steinberg, Observation of the nonlinear phase shift due to single post-selected photons, Nat. Phys. 11, 905 (2015).
- [12] B. Hacker, S. Welte, G. Rempe, and S. Ritter, A photo-nphoton quantum gate based on a single atom in an optical resonator, Nature (London) **536**, 193 (2016).
- [13] D. Tiarks, S. Schmidt-Eberle, T. Stolz, G. Rempe, and S. Dürr, A photon-photon quantum gate based on Rydberg interactions, Nat. Phys. **15**, 124 (2019).
- [14] J. P. Gaebler, T. R. Tan, Y. Lin, Y. Wan, R. Bowler, A. C. Keith, S. Glancy, K. Coakley, E. Knill, D. Leibfried, and D. J. Wineland, High-Fidelity Universal Gate Set for ⁹Be⁺ Ion Qubits, Phys. Rev. Lett. 117, 060505 (2016).
- [15] J. H. Shapiro, Single-photon Kerr nonlinearities do not help quantum computation, Phys. Rev. A 73, 062305 (2006).
- [16] J. Gea-Banacloche, Impossibility of large phase shifts via the giant Kerr effect with single-photon wave packets, Phys. Rev. A **81**, 043823 (2010).
- [17] K. Xia, M. Johnsson, P. L. Knight, and J. Twamley, Cavity-Free Scheme for Nondestructive Detection of a Single Optical Photon, Phys. Rev. Lett. **116**, 023601 (2016).
- [18] B. Viswanathan and J. Gea-Banacloche, Analytical results for a conditional phase shift between single-photon pulses in a nonlocal nonlinear medium, Phys. Rev. A 97, 032314 (2018).
- [19] N. K. Langford, S. Ramelow, R. Prevedel, W. J. Munro, G. J. Milburn, and A. Zeilinger, Efficient quantum computing using coherent photon conversion, Nature (London) 478, 360 (2011).
- [20] M. Y. Niu, I. L. Chuang, and J. H. Shapiro, Qudit-Basis Universal Quantum Computation Using $\chi^{(2)}$ Interactions, Phys. Rev. Lett. **120**, 160502 (2018).
- [21] A. Dot, E. Meyer-Scott, R. Ahmad, M. Rochette, and T. Jennewein, Converting one photon into two via four-wave mixing in optical fibers, Phys. Rev. A **90**, 043808 (2014).
- [22] Z.-Y. Liu, J.-T. Xiao, J.-K. Lin, J.-J. Wu, J.-Y. Juo, C.-Y. Cheng, and Y.-F. Chen, High-efficiency backward

^{*}Corresponding author.
stevensagona@gmail.com

†Corresponding author.
eden.figueroa@stonybrook.edu

‡S. S.-S. and R. S. contributed equally to this work.

^[1] G. Vallone, D. Bacco, D. Dequal, S. Gaiarin, V. Luceri, G. Bianco, and P. Villoresi, Experimental Satellite Quantum Communications, Phys. Rev. Lett. **115**, 040502 (2015).

^[2] S.-K. Liao *et al.*, Satellite-to-ground quantum key distribution, Nature (London) **549**, 43 (2017).

- four-wave mixing by quantum interference, Sci. Rep. 7, 15796 (2017).
- [23] Z.-Y. Liu, Y.-H. Chen, Y.-C. Chen, H.-Y. Lo, P.-J. Tsai, I. A. Yu, Y.-C. Chen, and Y.-F. Chen, Large Cross-Phase Modulations at the Few-Photon Level, Phys. Rev. Lett. 117, 203601 (2016).
- [24] See Supplemental Material at http://link.aps.org/supplemental/10.1103/PhysRevLett.125.243601 which covers the following topics: Experimental atomic scheme with connection to previous quantum memory experiments (sections I–II), theoretical model considering doppler and field quantization (III–V), homodyne reconstruction of quantum states and figures (VI–VIII), further considerations for atomic model, "quantum damage," and Gate operation (IX–XI), and tables of values obtained from MLE (Appendix C), and includes Refs. [25–40].
- [25] M. Fleischhauer and M.-D. Lukin, Dark-State Polaritons in Electromagnetically Induced Transparency, Phys. Rev. Lett. 84, 5094 (2000).
- [26] M. Namazi, C. Kupchak, B. Jordaan, R. Shahrokhshahi, and E. Figueroa, Ultralow-noise room-temperature quantum memory for polarization qubits, Phys. Rev. Applied 8, 034023 (2017).
- [27] J. Appel, A light-atom quantum interface based on electromagnetically induced transparency, doctoral thesis, University of Calgary, 2007 (unpublished), http://dx.doi.org/10 .11575/PRISM/1322.
- [28] J. Appel, E. Figueroa, D. Korystov, M. Lobino, and A.-I. Lvovsky, Quantum Memory for Squeezed Light, Phys. Rev. Lett. 100, 093602 (2008).
- [29] C. Kupchak, T. Mittiga, B. Jordaan, M. Namazi, C. Nlleke, and E. Figueroa, Room-temperature single-photon level memory for polarization states, Sci. Rep. 5, 7658 (2015).
- [30] M. Fleischhauer, A. Imamoglu, and J.-P. Marangos, Electromagnetically induced transparency: Optics in coherent media, Rev. Mod. Phys. 77, 633 (2005).
- [31] I. A. Fedorov, A. K. Fedorov, Y. V. Kurochkin, and A. I. Lvovsky, Tomography of a multimode quantum black box, New J. Phys. 17, 043063 (2015).

- [32] E. Figueroa, F. Vewinger, J. Appel, and A.-I. Lvovsky, Decoherence of electromagnetically induced transparency in atomic vapor, Opt. Lett. 31, 2625 (2006).
- [33] M. Rambach, A. Nikolova, T. J. Weinhold, and A. G. White, Sub-megahertz linewidth single photon source, APL Photonics 1, 096101 (2016).
- [34] H. Ogawa, H. Ohdan, K. Miyata, M. Taguchi, K. Makino, H. Yonezawa, J.-i. Yoshikawa, and A. Furusawa, Real-Time Quadrature Measurement of a Single-Photon Wave Packet with Continuous Temporal-Mode Matching, Phys. Rev. Lett. 116, 233602 (2016).
- [35] Z. Y. Ou, Complementarity and Fundamental Limit in Precision Phase Measurement, Phys. Rev. Lett. 77, 2352 (1996).
- [36] A. G. Fowler, M. Mariantoni, J. M. Martinis, and A. N. Cleland, Surface codes: Towards practical large-scale quantum computation, Phys. Rev. A. 86, 032324 (2012).
- [37] M. T. L. Hsu, G. Hétet, A. Peng, C. C. Harb, H.-A. Bachor, M. T. Johnsson, J. J. Hope, P. K. Lam, A. Dantan, J. Cviklinski, A. Bramati, and M. Pinard, Effect of atomic noise on optical squeezing via polarization self-rotation in a thermal vapor cell, Phys. Rev. A 73, 023806 (2006).
- [38] J. L. Everett, G. T. Campbell, Y.-W. Cho, P. Vernaz-Gris, D. B. Higginbottom, O. Pinel, N. P. Robins, P. K. Lam, and B. C. Buchler, Dynamical observations of self-stabilizing stationary light, Nat. Phys 13, 68 (2017).
- [39] A. V. Gorshkov, A. Andre, M. D. Lukin, and A. S. Sørensen, Photon storage in Λ-type optically dense atomic media. II. Free-space model, Phys. Rev. A 76, 033805 (2007).
- [40] A. I. Lvovsky, Iterative maximum-likelihood reconstruction in quantum homodyne tomography, J. Opt. B 6, S556 (2004).
- [41] M. Artoni and A. Zavatta, Large Phase-by-Phase Modulations in Atomic Interfaces, Phys. Rev. Lett. **115**, 113005 (2015).
- [42] A. I. Lvovsky and S. A. Babichev, Synthesis and tomographic characterization of the displaced Fock state of light, Phys. Rev. A 66, 011801(R) (2002).
- [43] A. I. Lvovsky and M. G. Raymer, Continuous-variable optical quantum-state tomography, Rev. Mod. Phys. 81, 299 (2009).